Displaying Sensed Tactile Cues with a Fingertip Haptic Device

Claudio Pacchierotti, Domenico Prattichizzo, and Katherine J. Kuchenbecker

Abstract—Telerobotic systems enable humans to explore and manipulate remote environments for applications such as surgery and disaster response, but few such systems provide the operator with cutaneous feedback. This article presents a novel approach to remote cutaneous interaction; our method is compatible with any fingertip tactile sensor and any mechanical tactile display device, and it does not require a position/force or skin deformation model. Instead, it directly maps the sensed stimuli to the best possible input commands for the device's motors using a data set recorded with the tactile sensor inside the device. As a proof of concept, we considered a haptic system composed of a BioTac tactile sensor, in charge of measuring contact deformations, and a custom 3-DoF cutaneous device with a flat contact platform, in charge of applying deformations to the user's fingertip. To validate the proposed approach and discover its inherent tradeoffs, we carried out two remote tactile interaction experiments. The first one evaluated the error between the tactile sensations registered by the BioTac in a remote environment and the sensations created by the cutaneous device for six representative tactile interactions and 27 variations of the display algorithm. The normalized average errors in the best condition were 3.0% of the BioTac's full 12-bit scale. The second experiment evaluated human subjects' experiences for the same six remote interactions and eight algorithm variations. The average subjective rating for the best algorithm variation was 8.2 out of 10, where 10 is best.

1 Introduction

Prior research has proven that haptic force feedback enhances the performance of robotic teleoperation systems in terms of task completion time [1], [2], [3], accuracy [2], [4], peak exerted force [5], [6], and average exerted force [3], [6], [7]. The human operator senses the feedback provided by traditional grounded haptic devices through two channels: cutaneous and kinesthetic [4], [8], [9], [10]. Cutaneous stimuli are detected by mechanoreceptors in the skin, enabling humans to recognize the local properties of objects such as shape, edges, and texture. Cutaneous perception for exploration and manipulation principally relies on measures of the location, intensity, direction, and timing of contact forces on the fingertips [9], [11]. On the other hand, kinesthesia provides humans with information about the position and velocity of neighboring body parts, as well as the applied force and torque, mainly by means of receptors in the muscles and joints [10], [12], [13].

Building on the success of kinesthetic force feedback, haptics researchers have recently focused great attention on cutaneous feedback. The richness of information that cutaneous receptors can detect, together with their broad distribution throughout the body, makes the skin an excellent communication channel [14]. Cutaneous feedback is known to play an important role in movement and weight perception [12], [15], [16], precision grasping [17], and shape recognition [18]. Cutaneous cues have even been found to be more informative than kinesthetic cues in curvature discrimination [19] and fine manipulation [20]. Moreover, cutaneous feedback can provide an elegant way to simplify the design of haptic interfaces: the low activation thresholds and high fingertip densities of cutaneous receptors [12], [14] enable researchers to design cutaneous display devices that are small, lightweight, and inexpensive, e.g., [16], [21], [22]. Cutaneous feedback has also recently been employed in teleoperation to provide the operator with haptic cues without causing instability [3], [4], [7].

An example of a cutaneous device exploiting these capabilities is the one presented by Minamizawa *et al.* [16], developed to display the weight of virtual objects. It consists of two motors that move a belt that is in contact with the user's fingertip. When the motors spin in opposite directions, the belt presses into the user's fingertip, while when the motors spin in the same direction, the belt applies a tangential force to the skin. This device was also used by Prattichizzo *et al.* [23] to display remote tactile experiences. Gleeson *et al.* [24] introduced a two-degree-of-freedom (2-DoF) cutaneous device that laterally stretches the skin of the fingertip using a 7 mm hemispherical tactor. Its two RC servo motors and compliant flexure stage can move the tactor along any path in the plane of the fingerpad. This device has been used to guide a human user navigating an unknown space [25].

Although these cutaneous devices have been successfully employed in various scenarios, their end-effectors *always* contact the fingerpad. They thus cannot provide the sensation of breaking and making contact with virtual and remote surfaces, cues that are known to be important to tactile interaction [13], [26]. Provancher *et al.* [27] designed the contact location display to overcome this limitation; it includes a roller that translates along as well as makes and breaks contact with the user's fingertip. Kuchenbecker *et al.* [21] employed a similar principle to create a non-actuated

- *C. Pacchierotti is with the Dept. of Information Engineering and Mathematics, University of Siena, Siena, Italy, with the Dept. of Advanced Robotics, Istituto Italiano di Tecnologia, Genova, Italy, and with the Depts. of Mechanical Engineering & Applied Mechanics and Computer & Information Science, GRASP Laboratory, University of Pennsylvania, Philadelphia, PA, USA. E-mail: pacchierotti@dii.unisi.it.*
- *D. Prattichizzo is with the Dept. of Information Engineering and Mathematics, University of Siena, Siena, Italy and with the Dept. of Advanced Robotics, Istituto Italiano di Tecnologia, Genova, Italy. E-mail: prattichizzo@dii.unisi.it.*
- *K. J. Kuchenbecker is with the Depts. of Mechanical Engineering & Applied Mechanics and Computer & Information Science, GRASP Laboratory, University of Pennsylvania, Philadelphia, PA, USA. E-mail: kuchenbe@seas.upenn.edu.*

- *This research has received funding from the European Union Seventh Framework Programme FP7/2007-2013 under grant n°601165 of the project "WEARHAP - WEARable HAPtics for humans and robots".*

fingertip device that makes contact with the user's skin when force feedback is applied. Frisoli *et al.* [28] achieved a similar effect by creating a finger-mounted thimble that moves a 5-DoF flat contact plate around the fingertip. The device can be also attached to the end-effector of a grounded haptic interface to combine the characteristics of an encounter-type haptic system with display of contact surface orientation. More recently, Pacchierotti *et al.* [3] presented a 3-DoF cutaneous device for remote tactile interaction. Its design is similar to the ones described in [8], [22], but it adds three springs to enable the platform to make and break contact with the fingertip. A modified version of this device will be also employed in this work.

Although these devices greatly improved the rendering of remote and virtual environments by displaying cutaneous sensations, they have all been employed in scenarios that treat the cutaneous interaction as a point force rather than spatially distributed sensations. The device presented by Kuchenbecker *et al.* [21], for example, is attached to a single-point grounded haptic device; Prattichizzo *et al.* [23] measured remote forces through only one force sensor; and the authors of [3], [8], [22] evaluated the virtual environment contact forces as though they were applied at one contact point. On the one hand, this simplified approach makes these haptic systems very easy to control, with only a few input parameters and simple force sensing systems. On the other hand, this approach cannot correctly represent the wide range of sensations the fingertip may encounter during a real interaction, since it does fully account for the spatial distribution of cutaneous receptors [12], [13].

Finally, most of the aforementioned devices make use of skin deformation models to determine the actuator inputs needed to apply a given force. For example, Pacchierotti *et al.* [3] used a simple isotropic elastic model of the fingertip, assuming a linear relationship between platform displacement and resultant wrench, while Gleeson *et al.* [24] characterized the interaction between their device and the skin through an experiment with seven human subjects. Although they have served well, such models do not guarantee accurate delivery of the desired force on the user's fingertip.

Motivated by these past investigations, this article presents a novel approach to remote tactile interaction. Our approach *directly* maps the remote sensed stimuli to input commands for the cutaneous device's motors, without using any kind of skin deformation model or force/position estimation. Instead, it employs a k-nearest-neighbor-based algorithm that uses a data set of tactile sensations recorded with the tactile sensor *inside* the device. Our approach is compatible with any fingertip sensing system and any mechanical tactile display device. Although nearest neighbor algorithms are widespread in other areas of research [29], [30], [31], to the best of our knowledge there is no prior evidence of their use in tactile rendering. Similarly, placing the tactile sensor inside the device to directly measure its outputs is similar to using a camera to assess the fidelity of a video display [32], [33], or using a microphone to assess the fidelity of an auditory output [34], [35]. Again, this approach is entirely new in touch display.

As a proof of concept, we considered a haptic system composed of a BioTac tactile sensor (SynTouch LLC, Los Angeles, USA), in charge of registering contact deformations at the remote site, and a custom 3-DoF cutaneous device, in charge of applying those deformations to the user's fingertip via a mobile platform. We validated the proposed approach by carrying out one objective and one subjective experiment with our proof-of-concept system. The key idea behind our approach and an elementary evaluation of its performance were presented in [36]. This article significantly extends our prior work by recording a new data set that is approximately 4.6 times larger than the previous one, by retrieving multiple neighbors of the point sensed by the BioTac to improve the algorithm's rendering accuracy, and by performing a comprehensive objective evaluation and a completely new subjective evaluation of the system's performance.

The rest of this article is organized as follows. Sec. 2 describes the haptic system and the algorithm that maps deformations registered by the tactile sensor onto appropriate input commands for the cutaneous device's motors. Secs. 3 and 4 present and discuss the results of our two validation experiments. Finally, Sec. 5 provides concluding remarks and perspectives on the future of this line of research.

2 Methods

We designed the proposed approach to work with any fingertip haptic system that includes mechanical sensing and mechanical actuation. As a proof of concept, we selected a BioTac sensor and a custom 3-DoF cutaneous device. This Section presents the haptic system and the proposed mapping algorithm.

2.1 Sensing and actuation systems

The BioTac tactile sensor mimics the physical properties and sensory capabilities of the human fingertip [37], [38]. As shown in Fig. 1a, it consists of three complementary sensory systems (deformation, internal fluid pressure, and temperature) integrated into a single package. Contact forces deform the elastic skin and the underlying conductive fluid, changing the impedances of 19 electrodes distributed over the surface of the rigid core. The DC pressure of the conductive fluid is measured by a hydro-acoustic pressure sensor, which also detects the AC pressure changes caused by transient contacts such as textures. The BioTac is internally heated to near human body temperature, and both DC and AC temperature are measured by a thermistor placed near the surface of the rigid core.

The haptic interface employed in this work is a 3-DoF fingertip cutaneous device that is similar to the one presented by Pacchierotti *et al.* [3]. As shown in Fig. 1b, it is composed of a static platform that houses three servo motors above the user's fingernail and a mobile platform that applies the requested stimuli to the fingertip. Three cables connect the two platforms, and springs around the cables keep the mobile platform in a reference configuration, away from the fingertip, when not actuated. By controlling the cable lengths, the motors can orient and translate the mobile platform in three-dimensional space. The device fastens to the finger with a fabric strap. The actuators used in our prototype are Sub-Micro Servo 3.7g motors (Pololu Corporation, Las Vegas, USA), which are able to exert up to 39 N·mm torque; they have a positioning resolution of $0.5°$, are controlled at 50 Hz, and can move $60°$ in 0.07 s. The motors were controlled through a PhidgetAdvancedServo

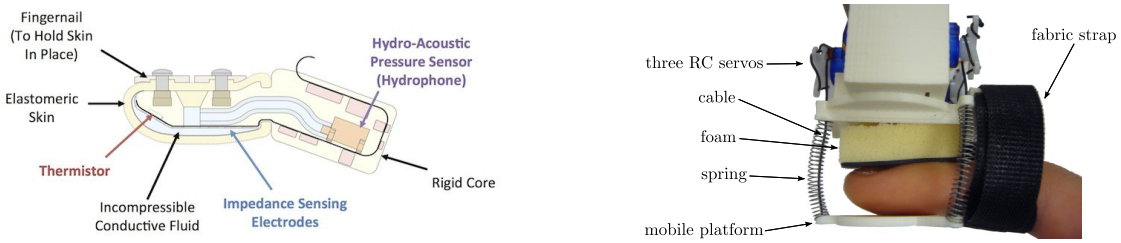

(a) The BioTac sensor (picture courtesy of SynTouch LLC)

(b) The 3-DoF cutaneous device

Fig. 1. The haptic system considered in this work includes a BioTac tactile sensor, in charge of registering contact deformations at the remote environment, and a custom 3-DoF cutaneous device, in charge of applying those deformations to the user's fingertip through a mobile platform controlled by three RC servos.

8-Motor board (Phidgets, Calgary, Canada). A short video showing the device is available as supplemental material.

From the 19 electrode impedances distributed over the BioTac's surface and the DC pressure of the conductive fluid, it is not trivial to control the orientation and position of the mobile platform to recreate the contact deformations applied to the sensor. Wettels *et al.* [39] first attempted to estimate the tangential stress applied to a BioTac using a Kalman Filter on the impedances registered by the electrodes. Later, Wettels *et al.* [37] used machine learning techniques to estimate the radius of curvature, point of application of force, and force vector from a BioTac during sensor-object interaction, but such methods work well only for interactions similar to those used during training. More recently, Jimenez and Fishel [40] presented a prosthetic hand equipped with a BioTac sensor. Contact force is fed back to the user's arm through a series of pneumatic air muscles driven by the fluid pressure of the BioTac; notably, this work did not make use of the electrode impedances, as the mapping to shape display is not obvious.

2.2 Mapping between remote sensed data and motor commands

Our goal is to enable the user to perceive, through the 3-DoF fingertip cutaneous device, the deformations experienced by the BioTac in the remote environment. In other words, we aim to find an effective many–to–few mapping between the rich sensory information provided by the BioTac and the limited actuation capabilities of the fingertip cutaneous device. Since our focus is in sensing deformations, we consider the 19 electrode impedance readings and the DC pressure signal. The BioTac senses these quantities at a rate of 100 Hz with a precision of 12 bits. Let $\boldsymbol{s(k)} \in \mathbb{S} = \{(s_1(k), \ldots, s_{20}(k)) \in \mathbb{Z}^{20} : 0 \leq s_i(k) \leq 4095\}$ be a vector containing the values sensed at instant k. In contrast, our cutaneous device uses three position-controlled motors. Let $\boldsymbol{m(k)} \in \mathbb{M} = \{(m_1(k), m_2(k), m_3(k)) \in \mathbb{R}^3 : 30° \leq m_i(k) < 195°\}$ be a vector containing the commanded angles for these motors at instant k. Note that we are neglecting quantization in the motor position outputs for simplicity. In order to simplify the notation further, the sampling time index k will be omitted from now on.

How can we map a given BioTac sensation to a congruent configuration of the mobile platform? Because the BioTac mimics the *physical* properties of the human fingertip [37], [38], we realized that we could place it inside the cutaneous device to discover how the motion of the mobile platform affects the tactile sensor. To the best of our knowledge, no other work in the literature takes a similar approach. As shown in Fig. 2, the BioTac was placed between the foam and the mobile platform, in the same way a human user would wear the device. We then moved the mobile platform to a wide range of configurations and registered the effect of each of these configurations on the BioTac, saving both the commanded motor angles $\boldsymbol{m_*}$ and the resulting effect on the tactile sensor $\boldsymbol{s_*}$. Using a moderate step size of $\theta = 3°$ yields $(\frac{195° - 30°}{3°})^3 = 166375$ unique platform configurations. The platform was held in each configuration for 0.1 s, and the values gathered by the BioTac were arithmetically averaged. Data collection took approximately 47 hours. At the end of data collection, we were thus able to evaluate the mapping function

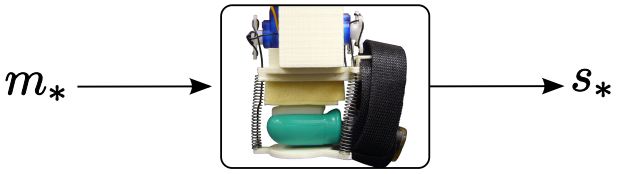

Fig. 2. Data collection. The BioTac was placed inside the cutaneous device, and the platform was moved to a wide range of configurations. The motor inputs $\boldsymbol{m_*}$ and the resultant cutaneous sensations $\boldsymbol{s_*}$ were recorded.

$$\begin{aligned} \mu &: \mathbb{S}_* \rightarrow \mathbb{M}_*, \\ \mu(\boldsymbol{s_*}) &= \boldsymbol{m_*}, \end{aligned} \tag{1}$$

which links the BioTac sensed data to the motor input commands. Set $\mathbb{M}_* \subset \mathbb{M}$ contains all the angle triplets actuated during data collection, and $\mathbb{S}_* \subset \mathbb{S}$ contains all the resulting sensed values registered by the BioTac. In this case the cardinality of sets $\mathbb{S}_*$ and $\mathbb{M}_*$ is 166375, which is much lower than the 4096^{20} different points the BioTac can sense (i.e., $|\mathbb{S}| = 4096^{20}$). Function $\mu(\cdot)$ is thus defined for a very small subset of all the possible tactile sensations the BioTac can experience. For this reason, we cannot simply deploy the sensor in a remote environment and expect its sensed points to be in the domain of our mapping function $\mu(\cdot)$. Unfortunately, this problem cannot be fixed by simply reducing the angle step size during data collection. The shape of the platform and the limited degrees of freedom of the cutaneous device will always couple the behavior of neighboring electrodes, so not all points in $\mathbb{S}$ are reachable

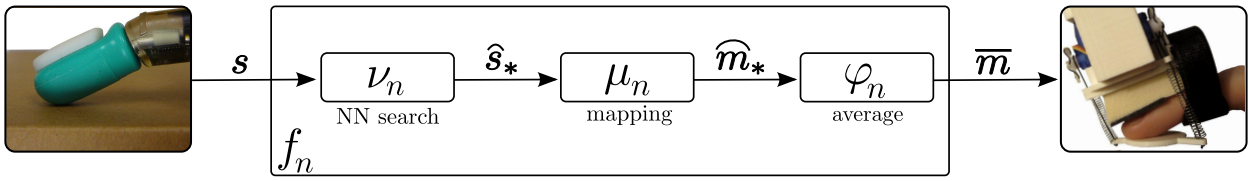

Fig. 3. Proposed algorithm. The BioTac registers a tactile sensation $\boldsymbol{s}$ at the remote environment. Function $\nu_n(\cdot)$ looks for the n closest points $\boldsymbol{s}_*$ contained in the set recorded during data collection. These points are then mapped by $\mu_n(\cdot)$ to the corresponding motor angle triplets $\boldsymbol{m}_*$. Finally, $\varphi_n(\cdot)$ averages those points to find the angle triplet $\overline{\boldsymbol{m}}$ that should be actuated by the device to allow the user to feel an approximation of what the BioTac is feeling.

with the given device. Other low-DoF cutaneous devices would be able to reach different subsets of $\mathbb{S}$.

We thus need a function that maps a *generic* sensed point $\boldsymbol{s} \in \mathbb{S}$ to one in our mapping function's domain $\mathbb{S}_*$. An idea, for example, is to look for the point in our domain closest to the sensed one, thus defining

$$\begin{aligned} &\nu : \mathbb{S} \rightarrow \mathbb{S}_*, \\ &\nu(\boldsymbol{s}) = \boldsymbol{s}_*, \end{aligned} \tag{2}$$

as the function that maps a generic point $\boldsymbol{s} \in \mathbb{S}$, sensed by the BioTac, to the closest one in $\mathbb{S}_*$. In this work we implemented the nearest point search using the Approximate Nearest Neighbour (ANN) C++ library by Mount and Arya [41], [42], considering the 20-dimensional Euclidean distance metric. The library stores set $\mathbb{S}_*$ into a k-d tree data structure, and then, given the query point $\boldsymbol{s}$, it retrieves the nearest point $\boldsymbol{s}_* \in \mathbb{S}_*$. Although the library supports the search for approximate nearest neighbors, we employed the exact search. In order to evenly weight the twenty elements of the sensed data when computing the distance, we divided each component of $\boldsymbol{s}$ and $\boldsymbol{s}_*$ by the corresponding standard deviation observed during data collection, so that the standard deviation of each component of the vectors in $\mathbb{S}_*$ becomes 1.

It is now trivial to combine functions $\mu(\cdot)$ and $\nu(\cdot)$ to define

$$\begin{aligned} &f : \mathbb{S} \rightarrow \mathbb{M}_*, \\ &f(\boldsymbol{s}) = \mu(\nu(\boldsymbol{s})) = \mu(\boldsymbol{s}_*) = \boldsymbol{m}_*, \end{aligned} \tag{3}$$

as our final function, which maps a generic point $\boldsymbol{s} \in \mathbb{S}$, sensed by the BioTac, to the motor angle triplet $\boldsymbol{m}_* \in \mathbb{M}_*$ that most closely causes sensation $\boldsymbol{s}$.

Although $f(\cdot)$ provides an effective way to map a generic point sensed by the BioTac to a motor angle triplet, its image set $\mathbb{M}_*$ contains a very small subset of all the possible angle configurations the motors can reach. Our $3°$ step size in data collection yielded only $\frac{195°-30°}{3°} = 54$ different angle configurations out of the $\frac{195°-30°}{0.5°} = 330$ configurations that each motor can reach. This problem can be easily addressed by choosing a smaller step size. However, considering that the present data collection took 47 hours, this approach may not always be feasible. A step size of $\theta = 0.5°$ (the servo angle resolution) would yield $(\frac{195°-30°}{0.5°})^3 \approx 3.6 \cdot 10^7$ unique platform configurations and an estimated duration of more than one year for data collection, which is not justified. Moreover, having so many points in $\mathbb{S}_*$ would also impose severe computational constraints on the algorithm speed.

An alternative way to address this problem is redefining our search function $\nu(\cdot)$ to provide more than one neighbor of the point sensed by the BioTac. The resulting motor angle triplets can then be combined using a weighted average. In addition to enlarging the image set of our final function, this approach also makes the system more robust to isolated errors during data collection. Let us thus define

$$\begin{aligned} &\nu_n : \mathbb{S} \rightarrow \mathbb{S}_*^n, \\ &\nu_n(\boldsymbol{s}) = \begin{bmatrix} \boldsymbol{s}_{*,1} \\ \boldsymbol{s}_{*,2} \\ \vdots \\ \boldsymbol{s}_{*,n} \end{bmatrix} = \hat{\boldsymbol{s}}_*, \end{aligned} \tag{4}$$

as our improved search function that maps a generic point $\boldsymbol{s} \in \mathbb{S}$, sensed by the BioTac, to the n closest ones in $\mathbb{S}_*$, and

$$\begin{aligned} &\mu_n : \mathbb{S}_*^n \rightarrow \mathbb{M}_*^n, \\ &\mu_n(\hat{\boldsymbol{s}}_*) = \mu_n\left(\begin{bmatrix} \boldsymbol{s}_{*,1} \\ \boldsymbol{s}_{*,2} \\ \vdots \\ \boldsymbol{s}_{*,n} \end{bmatrix}\right) = \begin{bmatrix} \mu(\boldsymbol{s}_{*,1}) \\ \mu(\boldsymbol{s}_{*,2}) \\ \vdots \\ \mu(\boldsymbol{s}_{*,n}) \end{bmatrix} = \\ &= \begin{bmatrix} \boldsymbol{m}_{*,1} \\ \boldsymbol{m}_{*,2} \\ \vdots \\ \boldsymbol{m}_{*,n} \end{bmatrix} = \widehat{\boldsymbol{m}}_*, \end{aligned} \tag{5}$$

as the function that maps those n points to their corresponding motor angle triplets registered during data collection.

We now require an additional step to map $\widehat{\boldsymbol{m}}_* \in \mathbb{M}_*^n$ to a single angle triplet for the servo motors. Let us then define

$$\begin{aligned} &\varphi_n : \mathbb{M}_*^n \rightarrow \mathbb{M}, \\ &\varphi_n(\widehat{\boldsymbol{m}}_*) = \varphi_n\left(\begin{bmatrix} \boldsymbol{m}_{*,1} \\ \boldsymbol{m}_{*,2} \\ \vdots \\ \boldsymbol{m}_{*,n} \end{bmatrix}\right) = \overline{\boldsymbol{m}}, \end{aligned} \tag{6}$$

as the function that averages the n angle triplets in $\widehat{\boldsymbol{m}}_*$ to yield a single one defined in the set of *all* the angle triplets reachable by our motors. This work used a simple inverse-distance weighted mean. We thus computed each component of $\overline{\boldsymbol{m}} = (\overline{m}_1, \overline{m}_2, \overline{m}_3)$ as

$$\overline{m}_i = \sum_{q=1}^{n} \frac{w_q \cdot m_{*,q,i}}{\sum_{p=1}^{n} w_p}, \quad i = 1, 2, 3, \tag{7}$$

where $m_{*,q,i}$ is the i-th component of $\boldsymbol{m}_{*,\boldsymbol{q}}$, and $w_q = (|\boldsymbol{s} - \boldsymbol{s}_{*,\boldsymbol{q}}|)^{-2}$ is the reciprocal of the square of the distance between the sensed point $\boldsymbol{s}$ and the q-th point closest to it in $\mathbb{S}_*$, as evaluated by $\nu_n(\cdot)$.

Finally, we can combine $\mu_n(\cdot)$, $\nu_n(\cdot)$ and $\varphi_n(\cdot)$ to define

$$f_n : \mathbb{S} \to \mathbb{M},$$
$$f_n(\boldsymbol{s}) = \varphi_n(\mu_n(\nu_n(\boldsymbol{s}))) = \varphi_n(\mu_n(\widehat{\boldsymbol{s}}_*)) = \tag{8}$$
$$= \varphi_n(\widehat{\boldsymbol{m}}_*) = \overline{\boldsymbol{m}},$$

as our enhanced final function, which maps a generic point $\boldsymbol{s} \in \mathbb{S}$, sensed by the BioTac, to a motor angle triplet $\overline{\boldsymbol{m}} \in \mathbb{M}$. It is worth noting that $\mu(\cdot)$ and $\nu(\cdot)$, defined respectively in (1) and (2), are particular cases of $\mu_n(\cdot)$ and $\nu_n(\cdot)$ for $n = 1$. Moreover, function $\varphi_n(\cdot)$ for $n = 1$ is the identity function, so $f(\cdot)$ defined in (3) is also a particular case of $f_n(\cdot)$ for $n = 1$.

The algorithm is summarized in Fig. 3. Its performance is expected to improve when one reduces the angle step size in data collection, increases the degrees of freedom of the device, and/or increases the number of neighbors retrieved by function $\nu_n(\cdot)$. A short video featuring the BioTac interacting with a remote environment and the cutaneous device driven according to this algorithm is available as supplemental material. The system shown in the video uses only one neighbor, as in (3) and in the preliminary version of the system presented in [36].

3 Experimental Evaluation

We evaluated the proposed algorithm by carrying out two remote tactile interaction experiments. The first experiment aims to quantitatively evaluate the error between the tactile sensations registered by the BioTac in the remote environment and the ones actuated by the cutaneous device. The second experiment aims to collect quantitative data regarding the experience of human subjects using our tactile system.

To enable us to compare their results, the two experiments used the same set of remote tactile experiences. We recorded video and tactile data during six different interactions between a stationary BioTac sensor and a flat metal surface that was moved by hand to touch the BioTac's fingertip in different ways. The experimental setup is shown in Fig. 4, and a short video featuring all the interactions is available as supplemental material. The first interaction, called *back-flat-back* in Fig. 4a, consists of making contact with the proximal part of the BioTac, then moving toward the finger pulp and returning to the back part of the finger. The second one, called *tip-flat-tip* in Fig. 4b, consists of making contact with the distal part of the BioTac, then moving toward the finger pulp and returning to the tip. The third one, called *left-flat-left* in Fig. 4c, consists of making contact on the left lateral side of the BioTac, then moving toward the finger pulp and returning to the left side. The fourth one, called *right-flat-right* in Fig. 4d, performs the same sequence of interactions on the right lateral side of the BioTac. The fifth one, called *flat* in Fig. 4e, consists of making contact with the finger pulp with the surface parallel to the sensor's nail. The last one, called *complex* in Fig. 4f, is a combination of the other five motions. Each interaction

(a) Back-flat-back interaction

(b) Tip-flat-tip interaction

(c) Left-flat-left interaction

(d) Right-flat-right interaction

(e) Flat interaction

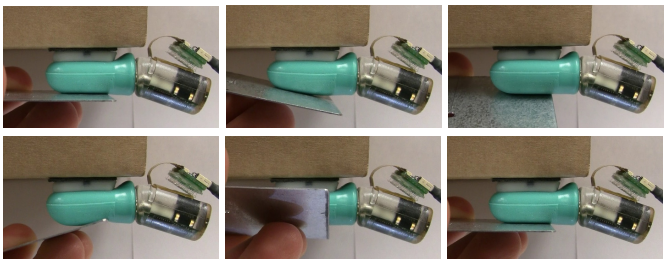

(g) Complex interaction (a combination of the others)

Fig. 4. Recorded interactions. We recorded video and tactile data during six different interactions between a BioTac sensor and a flat surface.

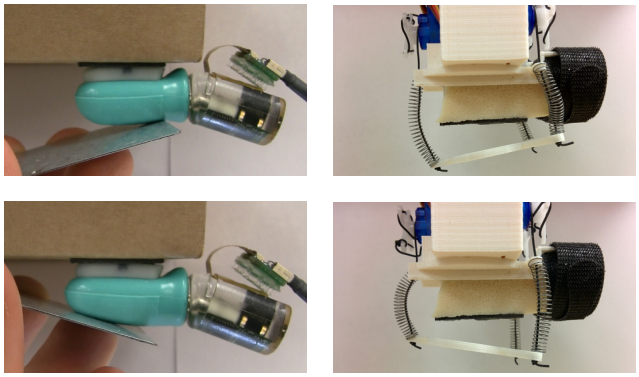

Fig. 5. Algorithm demonstration. Representative frames from the *back-flat-back* and *tip-flat-tip* videos, together with the respective platform configurations as chosen by the algorithm. The depicted cases used a step size of 3° and $n = 8$ neighbors.

was repeated three times within its recording. The whole tactile experience (six interactions, each of them repeated three times) lasts 3.4 minutes. Fig. 5 shows representative frames of the videos for the *back-flat-back* and *tip-flat-tip* interactions, together with the respective platform configurations chosen by the proposed algorithm. Note that the cutaneous device's platform mimics the relative orientation of the surface although our approach does not explicitly measure the surface's angle.

This twofold evaluation of our algorithm was inspired by similar approaches taken to evaluate the performance of rendering algorithms for other sensory modalities. The literature on compression algorithms for still pictures, for example, takes an approach very similar to ours. On the one hand, it objectively evaluates the quality of the compressed images by measuring the peak signal-to-noise ratio (PSNR) of the decoded image with respect to the original. On the other hand, it carries out subjective experiments where humans are asked to compare and rate the quality of the compressed images with respect to the original [43], [44], [45]. Similarly, researchers objectively evaluate the performance of compression algorithms for audio signals employing sophisticated ear models [46], [47], while the subjective evaluation requires human listeners to compare and rate the quality of the compressed audio signals with respect to the original [47], [48].

3.1 Objective evaluation

In order to evaluate the error between the tactile sensations registered in the remote environment and the ones actuated by the cutaneous device, we placed a BioTac sensor inside the cutaneous device, as done for data collection (see Fig. 2). We then sent the tactile data recorded during the six interactions of Fig. 4 through our algorithm and drove the cutaneous device to the resulting motor angle triplets over time, while recording what the BioTac sensed. A preliminary version of this experiment with a single tactile interaction was presented in [36].

We compared the results of nine different versions of the algorithm's parameters, varying the step size during data collection ($\theta = 3°, 6°, 9°$) and the number of points retrieved by the nearest neighbor function $\nu_n(\cdot)$, $n = 1, 4, 8$ (see (4)). Moreover, to show the generality of the algorithm, we also considered three different ways of controlling the cutaneous device: with one, two, or three degree of freedom. When controlling it as a 1-DoF device, we always command the three motors to the same target angle (i.e., $m_1 = m_2 = m_3$). While controlling it as a 2-DoF device, we give the two rear motors (the ones closer to the fabric strap) the same angle, and the front motor is driven independently. Reducing the degrees of freedom of the cutaneous device, as well as increasing the step size during data collection, reduces the cardinality of our reachable space $\mathbb{S}_*$. For example, a step size of 6° with a 2-DoF controller leads to $|\mathbb{S}_*| = 784$, while a step size of 9° with a 1-DoF controller leads to $|\mathbb{S}_*| = 19$. In order to guarantee the same setup for all of the conditions, we ran the data collection only once, considering a 3° step size and a 3-DoF configuration for the device, and from that we generated all of the required reachable spaces.

We tested all possible algorithm and device configurations for each of the six remote interactions of Fig. 4, ending

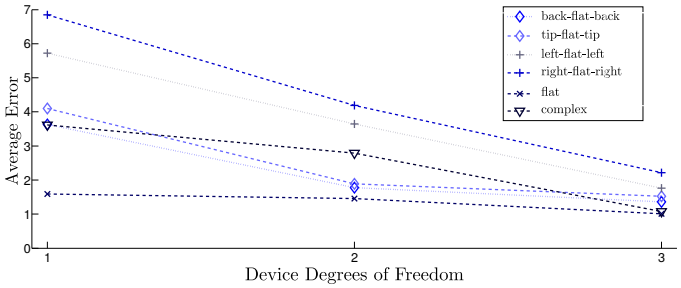

Fig. 6. Selected results from objective evaluation. Normalized error vs. degrees of freedom for each tactile interaction for a representative version of the algorithm ($n = 1$, $\theta = 3°$). While separated in this plot, the six tactile interactions were considered independent observations in the data analysis.

up with 3 (step size values) × 3 (nearest neighbor values) × 3 (DoF values) × 6 (interactions) = 162 different conditions. The experiment lasted 96 minutes. As a measure of fidelity, we calculated the error $\boldsymbol{e_f}$ between the tactile sensations registered by the BioTac in the remote environment $\boldsymbol{s}$ and the ones registered by the BioTac inside the cutaneous device $\boldsymbol{s_r}$. Then, we averaged the error across the 20 sensing channels and over time for each condition,

$$\bar{e}_f = \frac{1}{K}\sum_{k=1}^{K}\left(\sum_{i=1}^{20}\frac{|s_i - s_{r,i}|}{20}\right) \tag{9}$$

where K is the total number of samples recorded. As detailed in Sec. 2.2, the tactile sensations registered by the pressure sensor and the electrodes are normalized at runtime by dividing them by the corresponding standard deviation observed during data collection, so this error metric is also based on the normalized error.

Fig. 6 depicts the average normalized error versus device degrees of freedom for each type of interaction for a representative version of the algorithm ($n = 1$, $\theta = 3°$). One can see a general trend of lower errors with more degrees of freedom. Furthermore, the simplest interaction (*flat*) has approximately the same error for all versions of the device controller, while the motions that touch the sides of the BioTac have the highest errors and are most sensitive to controller version. Each datapoint in this plot represents just a single measurement, so we averaged the errors across the six interactions to enable statistical analysis. Fig. 7 shows the results averaged across the six tactile interactions. By examination of our recorded dataset and the kinematics of the cutaneous feedback device, we calculated that the lowest average error ($\bar{e}_f \approx 2.0$) corresponds to a platform orientation error of approximately 2.75° away from a nominal platform contact configuration, assuming no translation error. It is also useful to consider the average non-normalized error with respect to the full 12-bit scale the BioTac can reach (0 – 4095). The average error in the best condition (3-DoF, $\theta = 3°$, $n = 1$) was 3.0% of the full 12-bit scale, and it was 31.6% of full scale in the worst condition (1-DoF, $\theta = 9°$, $n = 1$).

To compare the different algorithm and device configurations, we ran a three-way repeated-measures ANOVA on the normalized error data shown in Fig. 7. Each tactile interaction was considered as an independent observation. Step size during data collection, number of neighbors retrieved

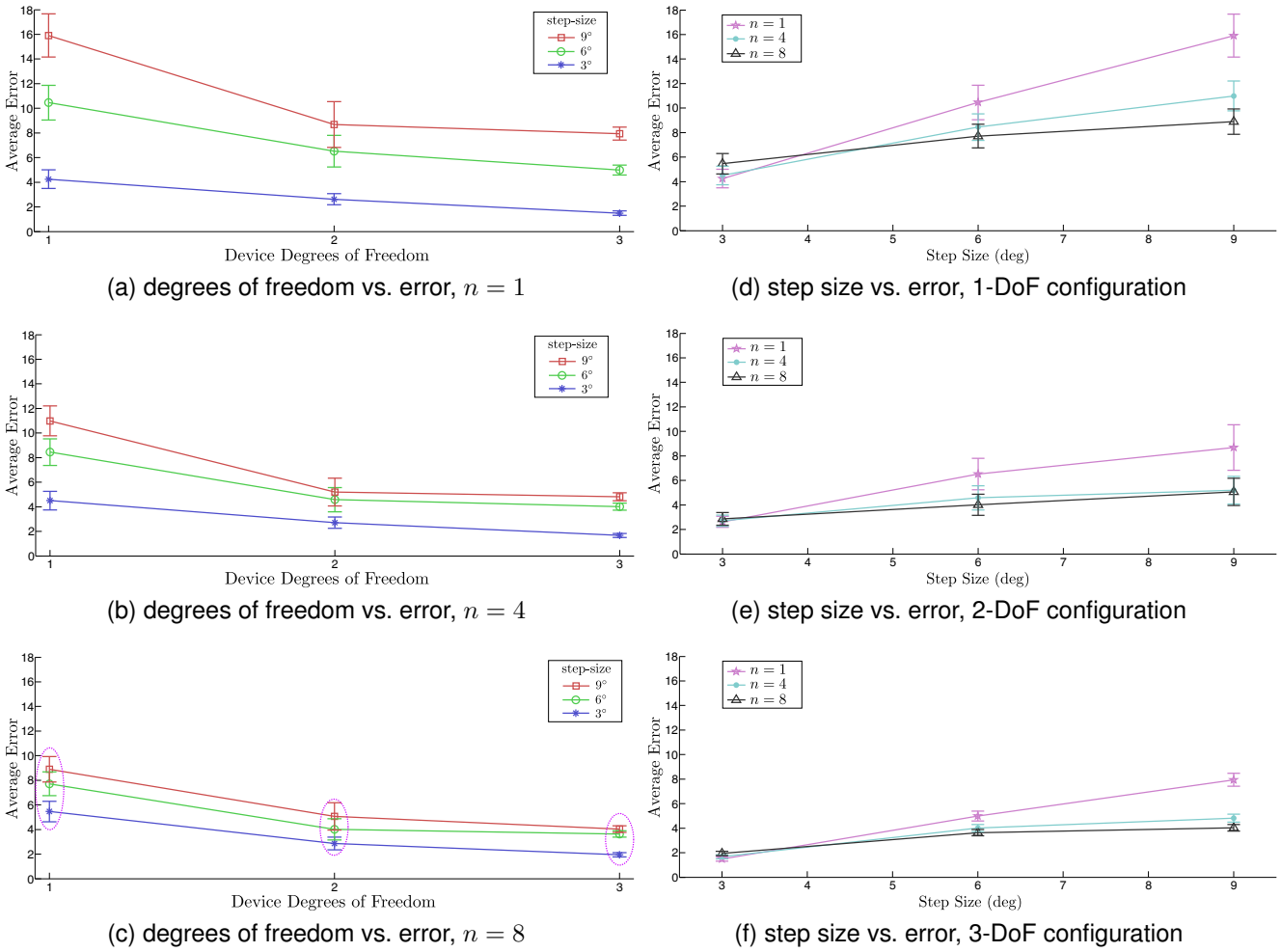

Fig. 7. Results of objective evaluation averaged across tactile interactions. Average normalized error vs. degrees of freedom (a, b, c) and step size (d, e, f) are reported (mean ± standard error of the mean). Statistical analysis revealed a significant increase in the rendering error when reducing the degrees of freedom of the cutaneous device, when increasing the step size during data collection, and when reducing the number of neighbors retrieved by function $\nu(\cdot)$. The dashed circles in Fig. 7c indicate the groups tested for equivalence using the two one-sided t-test (TOST).

by function $\nu(\cdot)$, and degrees of freedom of the device were treated as within-subject factors.

All the data passed the Shapiro-Wilk normality test. Mauchly's Test of Sphericity indicated that the assumption of sphericity had not been violated for the device degrees of freedom, while it was violated for the data collection step size ($\chi^2(2) = 17.008, p < 0.001$), number of neighbors retrieved ($\chi^2(2) = 21.705, p < 0.001$), interaction between degrees of freedom and step size ($\chi^2(9) = 40.938, p < 0.001$), interaction between degrees of freedom and number of neighbors retrieved ($\chi^2(9) = 38.852, p < 0.001$), and interaction between step size and number of neighbors retrieved ($\chi^2(9) = 44.385, p < 0.001$). A Greenhouse-Geisser correction was applied to the tests involving data that violate the sphericity assumption.

The ANOVA test revealed a statistically significant change in the error for degrees of freedom ($F(2, 10) = 31.415, p < 0.001$, partial $\eta^2 = 0.863$), step size ($F(1.007, 5.036) = 43.791, p = 0.001$, partial $\eta^2 = 0.898$), and number of neighbors retrieved ($F(1.002, 5.011) = 35.943, p = 0.002$, partial $\eta^2 = 0.878$). Moreover, there was a statistically significant interaction between degrees of freedom and step size ($F(1.146, 5.728) = 30.785, p = 0.001$, partial $\eta^2 = 0.860$), degrees of freedom and number of neighbors retrieved ($F(1.235, 6.177) = 25.528, p = 0.002$, partial $\eta^2 = 0.836$), and step size and number of neighbors retrieved ($F(1.016, 5.082) = 43.929, p = 0.001$, partial $\eta^2 = 0.898$). Post hoc analysis with Bonferroni adjustments revealed a significant increase in the rendering error when reducing the degrees of freedom of the cutaneous device (1-DoF vs. 2-DoF, $p = 0.013$; 1-DoF vs. 3-DoF, $p = 0.002$; 2-DoF vs. 3-DoF, $p = 0.036$), when increasing the step size during data collection (3° vs. 6°, $p = 0.005$; 3° vs. 9°, $p = 0.003$; 6° vs. 3°, $p = 0.002$), and when reducing the number of neighbors retrieved by function $\nu(\cdot)$ (1 vs. 4, $p = 0.006$; 1 vs. 8, $p = 0.005$; 4 vs. 8, $p = 0.013$). Table 1 summarizes the results of this statistical analysis.

As it is clear from Fig. 7 and from the statistical analysis reported above, there is a significant interaction between step size and number of neighbors retrieved by the algorithm: increasing the number of neighbors retrieved reduces the difference between conditions with dissimilar step sizes. To determine whether this difference can be considered statistically negligible, we used the two one-sided t-test approach (TOST). The null hypothesis of the TOST states that the mean values of two groups are different by at least

Three-way repeated-measures ANOVA	
Effect	p value
degrees of freedom	< 0.001
step size	0.001
number of neighbors	0.002
degrees of freedom × step size	0.001
degrees of freedom × number of neighbors	0.002
step size × number of neighbors	0.001

Post hoc analysis with Bonferroni	
degrees of freedom	p value
1-DoF vs. 2-DoF	0.013
1-DoF vs. 3-DoF	0.002
2-DoF vs. 3-DoF	0.036
step size	p value
3° vs. 6°	0.005
3° vs. 9°	0.003
6° vs. 3°	0.002
number of neighbors	p value
1 vs. 4	0.006
1 vs. 8	0.005
4 vs. 8	0.013

TABLE 1
Summary of the statistical analyses for the objective evaluation.

a certain amount ε. Then, in order to test for equivalence, the 90% confidence intervals for the difference between the two groups are evaluated. The null hypothesis that the groups differ by at least ε is rejected if the limits of the interval fall outside the $\pm\varepsilon$ bounds. Conversely, comparability is demonstrated when the bounds of the 90% confidence interval of the mean difference fall entirely within the $\pm\varepsilon$ bounds [49], [50]. The design of equivalence tests can be tricky because the acceptance criterion ε must be defined on the basis of prior knowledge of the measurement. For a sample data set of p independent measurements with standard deviation δ, for instance, ε must certainly be greater than $\delta/\sqrt{p}$, otherwise the test may fail simply because of imprecision, rather than because of a true difference. However, it must also be less than any specifications or standards that the testing is challenging, or the test becomes too easy and will not adequately discriminate.

In this work we evaluated ε as suggested in [50], where the authors provided a useful step-by-step process for performing equivalence testing with commonly available computational software packages. The two one-sided tests were performed between conditions retrieving $n = 8$ neighbors, considering separately conditions with different degrees of freedom. The three tested groups are circled in Fig. 7c. To avoid raising the family-wise error rate, i.e., the probability of at least one incorrectly rejected null hypothesis in a family of tests, we took into account the simple correction discussed in [51]. The tests revealed statistical equivalence between all three step sizes (3°, 6°, and 9°) when actuating one degree of freedom, and between 3° and 6° when actuating two and three degrees of freedom.

3.2 Subjective evaluation

We carried out a second experiment to evaluate the subjective experience of using the presented tactile system. We considered the same six tactile interactions used in Sec. 3.1, but we had to reduce the number of algorithm and device versions to keep the experiment to a reasonable duration for human subjects. Thus, we compared the two extreme step sizes (3° and 9°), the two extreme functions $\nu_n(\cdot)$ (retrieving 1 and 8 neighbors), and the two extreme ways of controlling the cutaneous device (one and three degrees of freedom). Similar to Sec. 3.1, we tested these conditions for each of the six remote interactions, ending up with 2 (step size values) × 2 (nearest neighbor values) × 2 (DoF values) × 6 (interactions) = 48 different conditions.

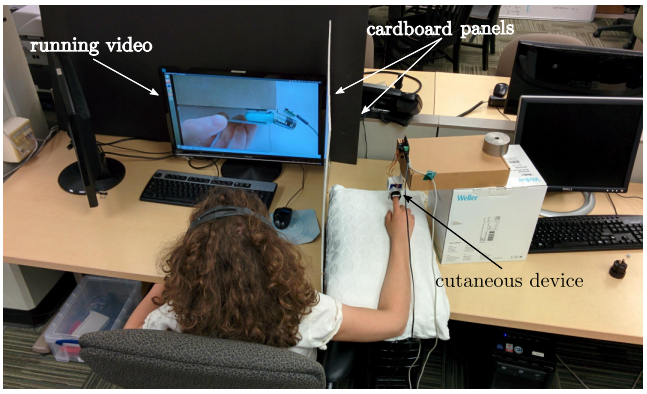

Fig. 8. Experimental setup for subjective evaluation. The subject was asked to wear the cutaneous device on his or her right index finger and watch videos featuring the six tactile interactions. At the end of each video, the subject rated how well the cutaneous device replicated the sensations experienced by the sensor in the video.

As shown in Fig. 8, the subject was asked to wear the cutaneous device on his or her right index finger and look at a 61-cm-diagonal LCD screen that presented the six tactile interaction videos shown in Fig. 4. Each video was played eight times, once for each considered combination of the algorithm parameters and the device controller. As the video played, the system sent the corresponding recorded tactile data through our algorithm and drove the cutaneous device accordingly, so that the subject felt on his or her finger a particular rendering of what the BioTac was experiencing in the video. Subjects were isolated from external noise through a pair of headphones playing white noise, and their vision of the cutaneous device was blocked by a cardboard panel. At the end of each video, the subject was asked to rate how well the cutaneous device replicated the sensations experienced by the sensor in the video. The response was given using a slider that ranged from 0 to 10, where a score of 0 meant "very badly" and a score of 10 meant "very well".

To determine the number of subjects needed for our research study, we ran a power analysis using the G*Power software. We estimated the effect size from the data retrieved in Sec. 3.1, expecting conditions showing higher errors in Sec. 3.1 to lead to lower subjective ratings in this experiment. Power analysis revealed that, in order to have a 90% chance of detecting differences in our data, we would need at least 10 participants (partial $\eta^2 = 0.836$, effect size 2.258, actual power 0.92). Because it is difficult to estimate a priori the correlation among repeated measures, we estimated power as though the measures were independent.

Ten participants took part in the experiment, including 4 women and 6 men. Two of them had previous experience with haptic interfaces. None of the participants reported any deficiencies in their visual or haptic perception abilities, and

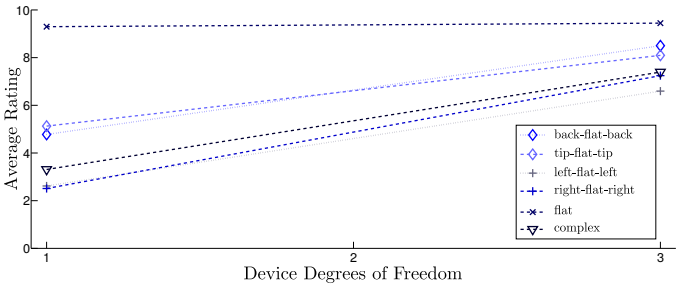

Fig. 9. Selected results from subjective evaluation. Degrees of freedom vs. rating for each tactile interaction for a representative configuration ($n = 1$, step size angle during data collection 3°).

all of them were right-hand dominant. The experimenter explained the procedures and spent about five minutes adjusting the setup to be comfortable before the subject began the experiment. Subjects consented to participate in this study under the University of Pennsylvania Institutional Review Board protocol #820095.

Fig. 9 shows the average rating vs. device degrees of freedom for each tactile interaction for a representative version of the algorithm ($n = 1$, $\theta = 3°$). One observes a general trend of higher ratings with more degrees of freedom. Furthermore, the simplest interaction (*flat*) has approximately the same rating for both versions of the device controller, while more complex interactions have lower ratings that are more sensitive to controller version. All of the results, averaged among tactile interactions, are shown in Fig. 10. In order to compare the different algorithm and device configurations, we ran a four-way repeated-measures ANOVA. Step size during data collection, number of neighbours retrieved by function $\nu(\cdot)$, device degrees of freedom, and type of tactile interaction were considered as within-subject factors. In contrast to the objective analysis presented in Sec. 3.1, it is important to note that we can consider the type of tactile interaction as a within-subject factor because we had ten independent measurements for each condition, rather than a single experiment.

Ratings were subjected to the arcsine square root transformation to stabilize variance [52]. All the transformed data passed the Shapiro–Wilk normality test and Mauchly's Test of Sphericity. Sphericity was assumed for variables with only two levels of repeated measures. The test revealed a statistically significant change in the rating due to device degrees of freedom ($F(1,9) = 2369.184, p < 0.001$, partial $\eta^2 = 0.996$), step size ($F(1,9) = 202.415, p < 0.001$, partial $\eta^2 = 0.957$), number of neighbors retrieved ($F(1,9) = 208.951, p < 0.001$, partial $\eta^2 = 0.959$), and type of tactile interaction ($F(5,45) = 198.972, p < 0.001$, partial $\eta^2 = 0.957$). Moreover, there was a statistically significant interaction between degrees of freedom and step size ($F(1,9) = 10.782, p = 0.009$, partial $\eta^2 = 0.545$), degrees of freedom and number of neighbors retrieved ($F(1,9) = 6.015, p = 0.037$, partial $\eta^2 = 0.401$), step size and number of neighbors retrieved ($F(1,9) = 88.307, p < 0.001$, partial $\eta^2 = 0.908$), degrees of freedom and tactile interaction ($F(5,45) = 66.824, p < 0.001$, partial $\eta^2 = 0.881$), and number of neighbors retrieved and tactile interaction ($F(5,45) = 5.268, p = 0.001$, partial $\eta^2 = 0.369$).

For the type of tactile interaction, post hoc analysis with Bonferroni adjustments revealed a significant difference in the rating of the *back-flat-back* interaction vs. *left-flat-left* ($p < 0.001$), *right-flat-right* ($p < 0.001$), *flat* ($p < 0.001$), and *complex* ($p = 0.007$) interactions; in the rating of the *tip-flat-tip* interaction vs. *left-flat-left* ($p < 0.001$), *right-flat-right* ($p < 0.001$), *flat* ($p < 0.001$), and *complex* ($p = 0.043$) interactions; in the rating of the *left-flat-left* interaction vs. *flat* ($p < 0.001$) and *complex* ($p = 0.007$) interactions; in the rating of the *right-flat-right* interaction vs. *flat* ($p < 0.001$) and *complex* ($p = 0.029$) interactions; and in the rating of the *flat* interaction vs. the *complex* ($p < 0.001$) interaction. Table 2 summarizes the results of this statistical analysis.

Four-way repeated-measures ANOVA	
Effect	p value
degrees of freedom	< 0.001
step size	< 0.001
number of neighbors	< 0.001
tactile interaction	< 0.001
degrees of freedom × step size	0.009
degrees of freedom × number of neighbors	0.037
step size × number of neighbors	< 0.001
degrees of freedom × tactile interactions	< 0.001
number of neighbors × tactile interactions	0.001

Post hoc analysis with Bonferroni	
tactile interactions	p value
back-flat-back vs. *left-flat-left*	< 0.001
back-flat-back vs. *right-flat-right*	< 0.001
back-flat-back vs. *flat*	< 0.001
back-flat-back vs. *complex*	0.007
tip-flat-tip vs. *left-flat-left*	< 0.001
tip-flat-tip vs. *right-flat-right*	< 0.001
tip-flat-tip vs. *flat*	< 0.001
tip-flat-tip vs. *complex*	0.043
left-flat-left vs. *flat*	< 0.001
left-flat-left vs. *complex*	0.007
right-flat-right vs. *flat*	< 0.001
right-flat-right vs. *complex*	0.029
flat vs. *complex*	< 0.001

TABLE 2
Summary of the statistical analyses for the subjective evaluation.

Similar to Sec. 3.1, this experiment also has a significant interaction between step size and number of neighbors retrieved by the algorithm: increasing the number of neighbors reduces the difference between conditions with dissimilar step sizes. To determine whether this difference can be considered statistically negligible, we used the two one-sided t-test (TOST) approach between conditions retrieving $n = 8$ neighbors, considering separately conditions with different degrees of freedom. The two tested groups are circled in Fig. 10b. We again evaluated the acceptance criterion ε as suggested in [50]. The tests revealed statistical equivalence between the 3° and 9° step sizes for both DoF values.

4 Discussion

We ran two experiments on remote tactile interaction. The objective experiment in Sec. 3.1 evaluated the error between the tactile sensations registered by the BioTac in the remote environment and the ones actuated by the cutaneous device

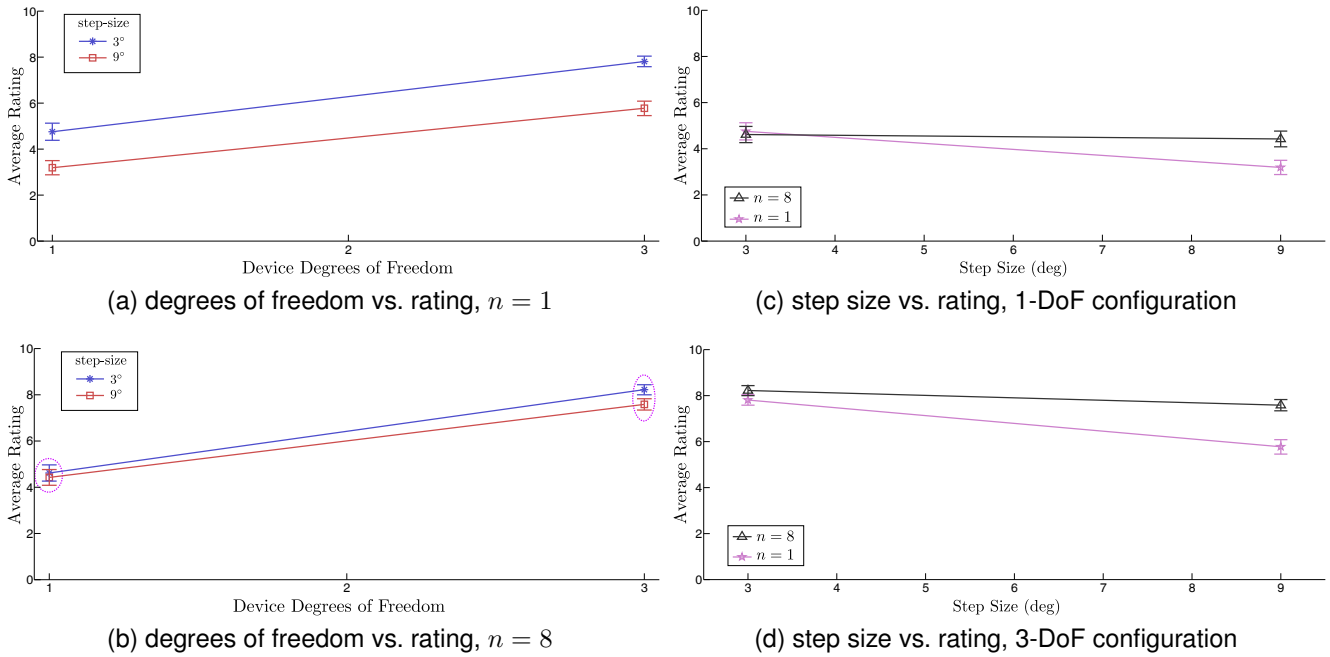

(a) degrees of freedom vs. rating, $n = 1$

(c) step size vs. rating, 1-DoF configuration

(b) degrees of freedom vs. rating, $n = 8$

(d) step size vs. rating, 3-DoF configuration

Fig. 10. Results of subjective evaluation averaged across tactile interactions. Degrees of freedom vs. rating (Figs. a, b, c) and step size vs. rating (Figs. d, e, f) are reported (mean $\pm$ standard error of the mean). Statistical analysis revealed a significant decrease of the user rating when reducing the degrees of freedom of the cutaneous device, when increasing the step size during data collection, and when reducing the number of neighbors retrieved by function $\nu(\cdot)$. The dashed circles in Fig. 10b indicate the groups tested for equivalence using the two one-sided t-test (TOST). These results agree with the findings of the objective evaluation, which are shown in Fig. 7.

for six tactile interactions and 27 algorithm and device configurations. The subjective experiment in Sec. 3.2 evaluated the quality of the human user's experience for the same six interactions and eight selected algorithm and device configurations. Both experiments showed improvements (lower errors or higher subjective ratings) when increasing the degrees of freedom of the cutaneous device, decreasing the step size during data collection, and increasing the number of neighbors retrieved by the search function.

Although it is clear that increasing the degrees of freedom of the cutaneous device leads to better performance, the improvement from 2-DoF to 3-DoF is not as marked as the one from 1-DoF to 2-DoF. This difference is clear from Figs. 7a, 7b, 7c, and the statistical analysis reported in Sec. 3.1. This fact can be explained by considering that three of the six tactile interactions do not require the use of the third degree of freedom (rotation around the long axis of the finger). This dependence on tactile interaction is clear from Fig. 6, where the average errors of the *back-flat-back*, *tip-flat-tip*, and *flat* interactions do not change much between the conditions with two and three degrees of freedom. Moreover, from the same figure, we can also notice how the average error of the *flat* interaction does not change much across all three DoF values; this result is expected because it is a 1-DoF interaction. A similar behavior can be also spotted in Fig. 9, where the subjective ratings of the *flat* interaction do not differ significantly between 1-DoF and 3-DoF.

A small step size guarantees fine search spaces $\mathbb{S}_*$ and $\mathbb{M}_*$, which was found to produce higher performance in terms of both mean error and user rating (see Figs. 7d, 7e, 7f and Figs. 10c, 10d, respectively). However, as highlighted in Sec. 2.2, the time needed to complete the data collection phase grows cubically with the inverse of the step size. For this reason, it is important to explore solutions guaranteeing adequate performance with coarser search spaces. This work investigated the possibility of interpolating within the motor space $\mathbb{M}_*$ by retrieving multiple neighbors of the sensed point. We hypothesized that this approach would reduce the need for a small step size, providing comparable performances at larger step sizes. From equality tests in Sec. 3.1 and 3.2, we can conclude that increasing the number of neighbors retrieved does mitigate the negative effect of choosing a large step size during data collection. This finding is also clear from Figs. 7a, 7b, 7c and Figs. 10a, 10b, where lines depicting different step sizes get closer to each other when increasing the number of neighbors retrieved. However, notice also that more neighbors retrieved means a higher run-time computational load.

Although it is clear that increasing the number of neighbors retrieved leads to improved performance, it is important to notice that this relationship is not linear. As we can see from Figs. 7a, 7b, 7c, the improvement from $n = 4$ to $n = 8$ is not as large as the one from $n = 1$ to $n = 4$. These diminishing returns are due to the fact that each neighbor is weighted according to the inverse of its squared distance from the sensed point (see (7)), and, therefore, each new neighbor counts less than all the preceding (closer) ones. It is also interesting to notice that retrieving more than one neighbor yields only a small improvement in performance, if any, for small step sizes: the 3° condition is similar across Figs. 7a, 7b, and 7c and across Figs. 10a and 10b. This constant level of performance probably stems from the fact that the motor space $\mathbb{M}_*$ is already fine enough for the given tactile experience and, thus, interpolating it is not necessary.

Turning our attention back to the six tactile interactions, we recall that the *flat* interaction was rated most highly by

subjects, as shown by Fig. 9 and the analysis of Sec. 3.2. Because this interaction matched the motion available from the 1-DoF device, it was rendered very well even when driving the three servo motors together (left side of Fig. 9). The performance of the other five interactions dramatically improved when the device used all three of its degrees of freedom (right side of Fig. 9). The post-hoc analysis of Sec. 3.2 showed that the *left-flat-left* and *right-flat-right* interactions performed significantly worse than the other tactile interactions. Four of the subjects also stated this opinion in their post-experiment questionnaire.

We believe the poor performance of *left-flat-left* and *right-flat-right* was caused by two main factors. The first reason is related to the distribution of the impedance-sensing electrodes on the surface of the BioTac core. Each side of the sensor includes only three electrodes, and we used Euclidean distance when looking for neighbors; consequently, the tactile sensations caused by platform contact on the sides of the BioTac may be less noticeable than tactile information from other types of interactions. The second factor centers on the shape of the platform and the positioning of the servo motors. During the data collection phase, we noticed that the selected cutaneous device struggles to apply pressure to only the lateral electrodes: the motor at the front of the device stimulates *all* the distal electrodes, while the two motors placed at the rear leave the distal lateral part of the BioTac untouched. If such interactions were important to the chosen task, one could design a tactile sensor and/or cutaneous device that were more adept at measuring and applying lateral contacts.

5 Conclusions and Future Work

This article presents a novel algorithm to map the cutaneous stimuli registered by a fingertip tactile sensor to the actions of a fingertip cutaneous haptic interface. The algorithm is compatible with any fingertip mechanical sensor and mechanical actuation system and does not use any kind of skin deformation model. Instead, it maps the sensed stimuli directly to the best input commands for the device's motors.

In order to validate the proposed approach, we carried out two remote tactile interaction experiments, employing a BioTac tactile sensor and a custom 3-DoF cutaneous device. The first experiment evaluated the error between the tactile sensations measured by the BioTac in a remote environment and the ones actuated by the cutaneous device for six remote tactile interactions and 27 algorithm and device configurations. The average error in the best condition was 3.0% of the full 12-bit scale the BioTac can reach, which is in agreement with the preliminary results reported in [36]. The second experiment evaluated the subjective experience of ten users for the same six interactions and eight selected algorithm and device configurations. The average rating for the best condition was 8.2 out of 10.

Although quite effective, this approach has a few limitations. For example, the output bandwidth is limited by the system sampling rate, the response speed of the motors, and the fact that the data set was collected during static conditions. Our approach does not use in fact any controller terms that respond to the *changes* in tactile sensations (i.e., how motor velocity affects tactile sensations over time), since we were interested in understanding how well this simpler quasi-static tracking approach would work. However, the amount of data required for our quasi-static approach is already very large, so it is not likely that one could collect a data set that sampled all motors for both position and velocity, as would be required to apply this approach to dynamic trajectories.

In the near future, we plan to embed a broad-bandwidth vibrotactile motor in the mobile platform, to enable the system to display vibration cues as well as fingertip deformation. The presented algorithm will need to be updated to take into account the AC signals detected by the BioTac's hydro-acoustic pressure sensor and then find a suitable transfer function between them and the vibrotactile motor's input signal. Moreover, we will update the mapping algorithm and experimental protocol to consider the dynamic behavior of the motor. We are also interested in augmenting our approach to compensate for variability in the size and shape of the fingertip among different users. We envision adding a user-specific calibration wherein the mobile platform of the device makes and breaks contact with the user's fingertip from many different angles. We will then shift the motor angles recorded during data collection so that the platform makes contact with the user's finger at the same time that the BioTac makes contact with the remote environment. Finally, we plan to incorporate our haptic system into a more complex robotic teleoperation system, wherein the BioTac senses the fingertip's tactile sensations at the slave side and the 3-DoF cutaneous device applies these sensations to the fingertip of the human operator. Applications range from robot-assisted surgery to fine manipulation and grasping. The proposed system seems particularly promising for medical scenarios, since cutaneous feedback can be employed in teleoperated medical procedures to provide the clinician with haptic cues without causing instability.

Acknowledgments

The authors thank Ian McMahon for his help in setting up the BioTac sensing system and Priyanka Shirsat for her help in realizing the cutaneous device. We also thank the anonymous reviewers for helping improve this manuscript.

References

[1] M. J. Massimino and T. B. Sheridan, "Teleoperator performance with varying force and visual feedback," *Human Factors: The Journal of the Human Factors and Ergonomics Society*, vol. 36, no. 1, pp. 145–157, 1994.

[2] L. Moody, C. Baber, T. N. Arvanitis *et al.*, "Objective surgical performance evaluation based on haptic feedback," *Studies in Health Technology and Informatics*, pp. 304–310, 2002.

[3] C. Pacchierotti, F. Chinello, M. Malvezzi, L. Meli, and D. Prattichizzo, "Two finger grasping simulation with cutaneous and kinesthetic force feedback," *Haptics: Perception, Devices, Mobility, and Communication*, pp. 373–382, 2012.

[4] D. Prattichizzo, C. Pacchierotti, and G. Rosati, "Cutaneous force feedback as a sensory subtraction technique in haptics," *IEEE Transactions on Haptics*, vol. 5, no. 4, pp. 289–300, 2012.

[5] B. Hannaford, "Task-level testing of the JPL-OMV smart end effector," in *Proc. Workshop on Space Telerobotics*, vol. 2, 1987.

[6] C. R. Wagner, N. Stylopoulos, and R. D. Howe, "The role of force feedback in surgery: analysis of blunt dissection," in *Proc. 10th Symposium of Haptic Interfaces for Virtual Environment and Teleoperator Systems*, 2002, pp. 68–74.

[7] L. Meli, C. Pacchierotti, and D. Prattichizzo, "Sensory subtraction in robot-assisted surgery: fingertip skin deformation feedback to ensure safety and improve transparency in bimanual haptic interaction," *IEEE Transactions on Biomedical Engineering*, vol. 61, no. 4, pp. 1318–1327, 2014.

[8] C. Pacchierotti, A. Tirmizi, and D. Prattichizzo, "Improving transparency in teleoperation by means of cutaneous tactile force feedback," *ACM Transactions on Applied Perception*, vol. 11, no. 1, pp. 4:1–4:16, 2014.

[9] I. Birznieks, P. Jenmalm, A. W. Goodwin, and R. S. Johansson, "Encoding of direction of fingertip forces by human tactile afferents," *The Journal of Neuroscience*, vol. 21, no. 20, pp. 8222–8237, 2001.

[10] V. Hayward, O. R. Astley, M. Cruz-Hernandez, D. Grant, and G. Robles-De-La-Torre, "Haptic interfaces and devices," *Sensor Review*, vol. 24, no. 1, pp. 16–29, 2004.

[11] K. O. Johnson, "The roles and functions of cutaneous mechanoreceptors," *Current Opinion in Neurobiology*, vol. 11, no. 4, pp. 455–461, 2001.

[12] B. B. Edin and N. Johansson, "Skin strain patterns provide kinaesthetic information to the human central nervous system." *The Journal of physiology*, vol. 487, no. Pt 1, pp. 243–251, 1995.

[13] B. B. Edin, L. Ascari, L. Beccai, S. Roccella, J.-J. Cabibihan, and M. Carrozza, "Bio-inspired sensorization of a biomechatronic robot hand for the grasp-and-lift task," *Brain Research Bulletin*, vol. 75, no. 6, pp. 785–795, 2008.

[14] R. S. Johansson and Å. B. Vallbo, "Tactile sensibility in the human hand: relative and absolute densities of four types of mechanoreceptive units in glabrous skin." *The Journal of Physiology*, vol. 286, no. 1, pp. 283–300, 1979.

[15] C. Giachritsis, R. Wright, and A. Wing, "The contribution of proprioceptive and cutaneous cues in weight perception: early evidence for maximum-likelihood integration," in *Haptics: Generating and Perceiving Tangible Sensations*, 2010, pp. 11–16.

[16] K. Minamizawa, S. Fukamachi, H. Kajimoto, N. Kawakami, and S. Tachi, "Gravity grabber: wearable haptic display to present virtual mass sensation," in *Proc. ACM Special Interest Group on Graphics and Interactive Techniques - Emerging Technologies*, 2007, pp. 8–es.

[17] G. Westling and R. Johansson, "Factors influencing the force control during precision grip," *Experimental Brain Research*, vol. 53, no. 2, pp. 277–284, 1984.

[18] J. Voisin, Y. Lamarre, and C. E. Chapman, "Haptic discrimination of object shape in humans: contribution of cutaneous and proprioceptive inputs," *Experimental Brain Research*, vol. 145, no. 2, pp. 251–260, 2002.

[19] M. W. A. Wijntjes, A. Sato, V. Hayward, and A. M. L. Kappers, "Local surface orientation dominates haptic curvature discrimination," *IEEE Transactions on Haptics*, vol. 2, no. 2, pp. 94–102, 2009.

[20] R. Johansson and G. Westling, "Roles of glabrous skin receptors and sensorimotor memory in automatic control of precision grip when lifting rougher or more slippery objects," *Experimental brain research*, vol. 56, no. 3, pp. 550–564, 1984.

[21] K. J. Kuchenbecker, D. Ferguson, M. Kutzer, M. Moses, and A. M. Okamura, "The Touch Thimble: providing fingertip contact feedback during point-force haptic interaction," in *Symposium on Haptic Interfaces for Virtual Environment and Teleoperator Systems*, 2008, pp. 239–246.

[22] D. Prattichizzo, F. Chinello, C. Pacchierotti, and M. Malvezzi, "Towards wearability in fingertip haptics: a 3-DoF wearable device for cutaneous force feedback," *IEEE Transactions on Haptics*, 2014, in Press.

[23] D. Prattichizzo, F. Chinello, C. Pacchierotti, and K. Minamizawa, "RemoTouch: a system for remote touch experience," in *Proc. of IEEE International Symposium on Robots and Human Interactive Communications*, 2010, pp. 676–679.

[24] B. T. Gleeson, S. K. Horschel, , and W. R. Provancher, "Design of a fingertip-mounted tactile display with tangential skin displacement feedback," *IEEE Transactions on Haptics*, vol. 3, no. 4, pp. 297–301, 2010.

[25] R. L. Koslover, B. T. Gleeson, J. T. de Bever, and W. R. Provancher, "Mobile navigation using haptic, audio, and visual direction cues with a handheld test platform," *IEEE Transactions on Haptics*, vol. 5, no. 1, pp. 33–38, 2012.

[26] G. Westling and R. S. Johansson, "Responses in glabrous skin mechanoreceptors during precision grip in humans," *Experimental Brain Research*, vol. 66, no. 1, pp. 128–140, 1987.

[27] W. R. Provancher, M. R. Cutkosky, K. J. Kuchenbecker, and G. Niemeyer, "Contact location display for haptic perception of curvature and object motion," *International Journal of Robotics Research*, vol. 24, no. 9, pp. 691–702, Sep. 2005.

[28] A. Frisoli, M. Solazzi, F. Salsedo, and M. Bergamasco, "A fingertip haptic display for improving curvature discrimination," *Presence: Teleoperators and Virtual Environments*, vol. 17, no. 6, pp. 550–561, 2008.

[29] S.-C. Tai, C. Lai, and Y.-C. Lin, "Two fast nearest neighbor searching algorithms for image vector quantization," *IEEE Transactions on Communications*, vol. 44, no. 12, pp. 1623–1628, 1996.

[30] J.-C. Wang, J.-F. Wang, K. W. He, and C.-S. Hsu, "Environmental sound classification using hybrid svm/knn classifier and mpeg-7 audio low-level descriptor," in *Proc. International Joint Conference on Neural Networks*, 2006, pp. 1731–1735.

[31] S. Salzberg and S. Cost, "Predicting protein secondary structure with a nearest-neighbor algorithm," *Journal of molecular biology*, vol. 227, no. 2, pp. 371–374, 1992.

[32] M. Brown, A. Majumder, and R. Yang, "Camera-based calibration techniques for seamless multiprojector displays," *IEEE Transactions on Visualization and Computer Graphics*, vol. 11, no. 2, pp. 193–206, 2005.

[33] A. Majumder, D. Jones, M. McCrory, M. E. Papka, and R. Stevens, "Using a camera to capture and correct spatial photometric variation in multi-projector displays," in *Proc. IEEE International Workshop on Projector-Camera Systems*, 2003.

[34] J. W. Fosgate and S. J. Wolfe, "Six-axis surround sound processor with automatic balancing and calibration," 1997, US Patent 5,666,424.

[35] M. LaBosco, "Loudspeaker calibration using multiple wireless microphones," 2012, uS Patent App. 13/564,805.

[36] C. Pacchierotti, D. Prattichizzo, and K. J. Kuchenbecker, "A data-driven approach to remote tactile interaction: from a BioTac sensor to any fingetip cutaneous device," in *Haptics: Neuroscience, Devices, Modeling, and Applications. Part I. Eurohaptics 2014*, ser. Lecture Notes in Computer Science, 2014, pp. 418–424.

[37] N. Wettels and G. E. Loeb, "Haptic feature extraction from a biomimetic tactile sensor: force, contact location and curvature," in *Proc. IEEE International Conference on Robotics and Biomimetics*, 2011, pp. 2471–2478.

[38] J. A. Fishel and G. E. Loeb, "Sensing tactile microvibrations with the BioTac–comparison with human sensitivity," in *Proc. IEEE RAS & EMBS International Conference on Biomedical Robotics and Biomechatronics*, 2012, pp. 1122–1127.

[39] N. Wettels, A. R. Parnandi, J.-H. Moon, G. E. Loeb, and G. Sukhatme, "Grip control using biomimetic tactile sensing systems," *IEEE/ASME Transactions on Mechatronics*, vol. 14, no. 6, pp. 718–723, 2009.

[40] M. C. Jimenez and J. A. Fishel, "Evaluation of force, vibration and thermal tactile feedback in prosthetic limbs," in *Proc. IEEE Haptics Symposium (HAPTICS)*, 2014, pp. 437–441.

[41] D. M. Mount and S. Arya. (2010) ANN: A Library for Approximate Nearest Neighbor Searching. https://web.archive.org/web/20131002094044/http://www.cs.umd.edu/~mount/ANN/.

[42] S. Arya and D. M. Mount, "Approximate nearest neighbor queries in fixed dimensions." in *ACM-SIAM Symposium on Discrete Algorithms*, vol. 93, 1993, pp. 271–280.

[43] F. De Simone, L. Goldmann, V. Baroncini, and T. Ebrahimi, "Subjective evaluation of JPEG XR image compression," in *SPIE Optical Engineering+ Applications*, 2009, pp. 74 430L–74 430L.

[44] D. Santa-Cruz, R. Grosbois, and T. Ebrahimi, "JPEG 2000 performance evaluation and assessment," *Signal Processing: Image Communication*, vol. 17, no. 1, pp. 113–130, 2002.

[45] G. Schaefer, R. Starosolski, and S. Y. Zhu, "An evaluation of lossless compression algorithms for medical infrared images," in *IEEE Engineering Medical Biological Conference*, 2005, pp. 1673–1676.

[46] T. Thiede, W. C. Treurniet, R. Bitto, C. Schmidmer, T. Sporer, J. G. Beerends, and C. Colomes, "PEAQ-The ITU standard for objective measurement of perceived audio quality," *Journal of the Audio Engineering Society*, vol. 48, no. 1/2, pp. 3–29, 2000.

[47] G. Vercellesi, A. Vitali, and M. Zerbini, "Mp3 audio quality for single and multiple encoding," in *Proc. IEEE International Conference on Multimedia and Expo*, 2007, pp. 1279–1282.

[48] I. Recommendation, "Method for the subjective assessment of intermediate quality level of coding systems," *ITU-R BS.1534-1*, 2003.

[49] C. Chen, N. Rathore, W. Ji, and A. Germansderfer, "Statistical equivalence testing for assessing bench-scale cleanability," *BioPharm International*, vol. 23, no. 2, 2010.

[50] G. B. Limentani, M. C. Ringo, F. Ye, M. L. Bergquist, and E. O. McSorley, "Beyond the t-test: statistical equivalence testing," *Analytical Chemistry*, vol. 77, no. 11, pp. 221–226, 2005.

[51] C. Lauzon and B. Caffo, "Easy multiplicity control in equivalence testing using two one-sided tests," *The American Statistician*, vol. 63, no. 2, pp. 147–154, 2009.

[52] C. L. Olson, "On choosing a test statistic in multivariate analysis of variance." *Psychological Bulletin*, vol. 83, no. 4, p. 579, 1976.

Domenico Prattichizzo (S'93 - M'95) received the Ph.D. degree in Robotics and Automation from the University of Pisa in 1995. Since 2002 he is an Associate Professor of Robotics at the University of Siena and since 2009 he is a Scientific Consultant at Istituto Italiano di Tecnoloogia. In 1994, he was a Visiting Scientist at the MIT AI Lab. Since 2014, he is Associate Editor of Frontiers of Biomedical Robotics. From 2007 to 2013 he has been Associate Editor in Chief of the IEEE Transactions on Haptics. From 2003 to 2007, he has been Associate Editor of the IEEE Transactions on Robotics and IEEE Transactions on Control Systems Technologies. He has been Chair of the Italian Chapter of the IEEE RAS (2006-2010), awarded with the IEEE 2009 Chapter of the Year Award. Research interests are in haptics, grasping, visual servoing, mobile robotics and geometric control. He is currently the Coordinator of the IP collaborative project "WEARable HAPtics for Humans and Robots" (WEARHAP).

Katherine J. Kuchenbecker (S'04 – M'06) received the B.S., M.S., and Ph.D. degrees in mechanical engineering from Stanford University, Stanford, CA, in 2000, 2002, and 2006, respectively. She completed a Postdoctoral Research Fellowship at the Johns Hopkins University, Baltimore, MD, in 2006–2007. She is currently an Associate Professor in Mechanical Engineering and Applied Mechanics at the University of Pennsylvania, Philadelphia. Her research centers on the design and control of haptic interfaces and robotic systems, and she directs the Penn Haptics Group, which is part of the General Robotics, Automation, Sensing, and Perception (GRASP) Laboratory. Prof. Kuchenbecker was the recipient of the 2009 National Science Foundation CAREER Award, the 2008 and 2011 Citations for Meritorious Service as a Reviewer for the IEEE Transactions on Haptics, and the 2012 IEEE Robotics and Automation Society Academic Early Career Award. She is co-chairing the IEEE Haptics Symposium in 2016 and 2018, and she is presently a co-chair of the IEEE RAS Technical Committee on Haptics.

Claudio Pacchierotti (S'12) received the B.S. and M.S. degrees cum laude in computer science from the University of Siena, Italy in 2009 and 2011, respectively. He received a Ph.D. degree in Robotics from the University of Siena in 2014. He was an exchange student at the Karlstad University in 2010, at the University of Padua in 2012, and at the University of Twente in 2013. He spent the first seven months of 2014 visiting the Penn Haptics Group at the University of Pennsylvania, Philadelphia, USA, which is part of the General Robotics, Automation, Sensing, and Perception (GRASP) Laboratory. He is currently a Postdoctoral researcher at the Dept. of Advanced Robotics of the Italian Institute of Technology. His research deals with robotics and haptics, focusing on cutaneous feedback techniques, wearable devices, and haptics for robotic surgery.